science.sciencemag.org/content/367/6475/272/suppl/DC1

Supplementary Materials for

A high-resolution summary of Cambrian to Early Triassic marine invertebrate biodiversity

Jun-xuan Fan, Shu-zhong Shen*, Douglas H. Erwin, Peter M. Sadler, Norman MacLeod, Qiu-ming Cheng, Xu-dong Hou, Jiao Yang, Xiang-dong Wang, Yue Wang, Hua Zhang, Xu Chen, Guo-xiang Li, Yi-chun Zhang, Yu-kun Shi, Dong-xun Yuan, Qing Chen, Lin-na Zhang, Chao Li, Ying-ying Zhao

*Corresponding author. Email: szshen@nju.edu.cn

Published 17 January 2020, *Science* **367**, 272 (2020)
DOI: 10.1126/science.aax4953

This PDF file includes:

Materials and Methods

1. Preparation and standardization of the stratigraphic data

Data compilation and standardization were conducted through the Geobiodiversity Database (*15*) from 2013 to 2017. The raw dataset contained 266,110 local Cambrian to Triassic records (i.e., first and last appearance levels) of 45,318 taxonomic units from 3,766 published stratigraphic sections (fig. S1). These were collected from all major Chinese tectonic plates. The authors spent three years verifying the taxonomic assignments into a consistent paleontological taxonomic classification system. This task resulted in 16,704 opinion records which have been attached to the raw data in the database. All taxonomic names in open nomenclature, such as cf. (~5752 records), sp. (~8016 records), aff. (~741 records), ex gr. (~232 records), or question marks (~2642 records) were removed from the dataset. Identifications to genus or higher taxonomic ranks were also omitted to ensure the data focused only on the reconstruction of species-level evolutionary history. All non-marine fossil groups (e.g., plants, vertebrates, pollen, spores) were also removed. Species recovered from only a single locality were removed after a few test calculations in order to partially standardize the sampling and research efforts and avoid the "monograph effect" (*64*). The final dataset retained after all standardization procedures included 116,060 local records of the stratigraphic ranges of 11,268 species in 3112 published stratigraphic sections. These data are publicly available through the OneStratigraphy (http://onestratigraphy.ddeworld.org/download/525dcacb35e44dc0b273549324a26087) and Dryad (*61*).

Most of the 3112 Paleozoic sections are distributed on the major Chinese tectonic plates, including South China, North China, Tarim, Chaidamu, tectonic blocks in Tibet, Cimmerian blocks etc., and also parts of the Indochina and Kazakhstan plates (fig. S2). During the Paleozoic these plates were situated across a wide range of paleolatitudes stretching from southern peri-Gondwanan to northern Boreal realms; the position of many plates changed considerably through the Paleozoic (fig. S3).

China, especially South China, is considered a paleobiodiversity center during the Paleozoic (*65*), and is suitable for multiclade analysis for two reasons. First, there are many key sections which cover quite long stratigraphic intervals and have yielded abundant, well-studied faunas that include many different fossil groups. For example, many Carboniferous and Permian sections contained many different formations representing a wide array of sedimentary settings that yielded both planktonic and benthic faunas.

Figure S4A shows the distribution of each fossil group in the studied sections, i.e., the number of sections for all fossil groups. The most abundant fossil group, Brachiopoda, occurs in 1162 sections. The seven most abundant fossil groups, occur in 354 to 1162 sections and provide strong biostratigraphic links among the 3112 sections. The richness of this dataset, in terms of its faunal content, regional dispersion and stratigraphic detail, makes it ideally suited for the construction of the Paleozoic biodiversity history.

Figure S4B shows the distribution frequency of fossil groups in sections. A total of 1343 sections contain one fossil group only. Approximately 57 percent of these

sections yielded at least two fossil groups. The considerable range of co-occurrences of different fossil groups is what makes it possible to assemble a composite standard reference section based on multi-clade data.

2. CONOP.SAGA correlation and composite section assembly

Most previous studies of taxonomic diversity of Paleozoic were limited by the relatively coarse time resolution of their data, generally 8 to 10 Myr (*1, 4, 12, 35*). We employed the constrained optimization (CONOP) compositing method of Sadler and Cooper (*19*; also see *21*) to reconstruct the Paleozoic biodiversity history of marine life, as this can provide much higher temporal resolutions by taking advantage of the information present in multiple correlatable stratigraphic sections [e.g., 37 kyr in the graptolite evolutionary study of Crampton et al. (*66*)]. Our initial estimates indicated that, in a standard CONOP implementation, calculations for data from about 10,000 species would take ca. 50 to 60 years. Our solution to this problem was to employ parallel computing and high-performance computing to increase the calculation rate. It is noteworthy that edge effects (usually a few Myr, Fig. 1A, gray bars on either side) in the two ends of the curve are present, but these are only a very small part on the two ends of the curve comparing to the entire Paleozoic and do not impact the main conclusions.

The original CONOP program was based on a simulated annealing algorithm and did not support either parallel computing or high-performance computing. We designed a special hybrid algorithm that combined simulated annealing and a genetic algorithm to overcome these limitations. The new program based on our hybrid implementation, CONOP.SAGA, was developed in 2017 with the Message Passing Interface technique using the C++ programming language. The program and source code are publicly available through the OneStratigraphy (http://onestratigraphy.ddeworld.org/download/525dcacb35e44dc0b273549324a26087) and Dryad (*61*) repositories. Its speed ratio is 0.5 to 0.6 per CPU core, an acceleration of 50x to 60x based on 100 CPU cores. Calculations for our investigation were conducted using 18,000 CPU cores on the "Tianhe-II" supercomputer, one of the fastest supercomputers in the world (https://www.top500.org/). To obtain robust results, we created a medium-sized dataset and made more than 10 complete CONOP.SAGA calculations. If the results are similar for each run, it suggests that the true global optimal solution has been found. Basic settings of the CONOP.SAGA parameters for the full dataset were estimated from these results. We then uploaded the full dataset and ran it while varying these parameters. Each calculation took 20 to 60 hours and produced one composite from the data set of 11,268 species. Ideally, the more times the procedure is run, the more robust results will get (*21*). However, this is costly on a supercomputer. To test the quality of our result we repeated our calculations three times with 1.2 billion iterations per run. All the three solutions are highly correlated (>98.6%), and differences in misfits (measurement of optimization) are even less than 0.5 percent. Total computation costs for the "Tianhe-II" supercomputer during the programming and final calculations were over 7,000,000 core hours.

In order to speed these calculation, we used the biostratigraphic framework of Gradstein et al. (*67*) and Cohen et al. (*24*). Zone-defining species were picked and assembled into a Paleozoic virtual section. To avoid any stratigraphic resolution issues and controversies over the definition of zonal species, we picked only one species from every 2 to 4 zone-defining species, so that stratigraphic range overlaps and/or reversals would be reduced. A total of 140 zonal species were employed to constrain biozone assignments in the virtual section (table S1). First and last appearances of the same species were set at the same level in the virtual section to minimize the ranges of zonal species, which will avoid any overestimation of the ranges of zonal species. The first appearances of zonal species were associated with high weights (e.g., 900,000) so that the best solution could be approximated much faster than would be the case for an unweighted or slightly weighted dataset. The virtual section was included as an independent section in the dataset for CONOP.SAGA analysis. Because the first appearances of these zone-defining species are highly regarded by most biostratigraphers, we gave these a higher weight (900,000) in the overall analysis. As a result, our best solution could be approximated much faster than would have been the case for an unweighted dataset.

3. Calibration of the composite to the geologic time

The composite section was calibrated to the geological time scales (*24, 67*) with updates published in the International Chronostratigraphic Chart v2018/8. We also used recently published dates based on new tracers around the Permian–Triassic boundary (e.g., *25, 34*). Geological ages corresponding to the base boundaries of 70 widely-recognized biozones were taken from published geologic time scales (fig. S5 and table S2) (*67*).

The calibrated composite is composed of 11,326 discrete temporal levels over an estimated interval from 538.85 Ma to 244.41 Ma. Accepting these figures as accurate, this yields a temporal resolution of ~26.0±14.9 kyr. The very fine resolving power of our analysis achieves is a matter of estimating the duration of the total stratigraphic interval studied — including boundary-date uncertainties — and dividing it by the number of separate events resolved, not the uncertainty in assigning an age to any stratigraphic boundary. A detailed description of the method used to calculate this estimate can be found in Sadler et al. (*14*). As new radioisotopic dates (and uncertainties) become available this information can be incorporated into our calibration, but it is very unlikely the total interval mean resolution will change substantially. However, mean resolutions for different subintervals are uneven (table S3), reflecting the effect of relatively uneven sampling efforts for different geological periods. For example, it is 64.46 kyr for the Cambrian, but 10.89 kyr for the Ordovician, which indicates the relatively fewer sampling levels in the Cambrian, but nearly five times more in the Ordovician.

4. Construction of unbinned diversity curve and its standardization based on sliding bin calculation technique

Based on the calibrated composite sequence of 11,268 species datums, we generated an unbinned diversity curve. All first and last appearance events in the composite were ranked by their geologic ages estimated via linear interpolation. The initial diversity value was set to zero. If the next event was a first appearance, the diversity was increased by one. If the next event was a last appearance, the diversity was decreased by one. Thus, calculation was based only on faunal changes rather than counts of species of across any time interval (binned diversity). This unbinned diversity calculation avoids bias due to uneven timescale subdivision. These unbinned diversity values were then sequenced by estimated age and assembled to produce a diversity-history curve for the Cambrian to Early Triassic interval (Fig. 1A, black line). The genus diversity curve was created by tracking the genus-level faunal changes using the same method (Fig. 1A, blue line).

Uncertainty estimates on the diversity rate curves were derived by bootstrapping the data, using species as the units of resampling, with 500 bootstrap iterations at each level of the composite (*20*; Fig. 1A). This separates peaks from adjacent troughs at two standard deviations, which approximates a 0.025 *p*-value under the assumption that these values are distributed normally.

The unbinned species diversity curve (Fig. 1A) was also standardized using a sliding bin calculation technique (fig. S6). The species diversity can be divided by the number of sections at each counting point, which will create a per-section diversity. However, the raw value of this index always overestimates the effect of sampling efforts. To avoid this bias, we created a new method of standardization to reveal the impact of uneven sampling on diversity estimation.

As the main point of our contribution lies in demonstrating how the CONOP.SAGA procedure can be used create high-resolution biodiversity curves based on paleontological data, we caution readers not to over-interpret the pattern of our biodiversity estimate. Ours is an estimate of raw biodiversity; the number of species and genus records that have been observed in the sections comprizing our dataset. We have taken simple steps to compensate for obvious sources of bias. But we do not regard this curve to be completely free of all sources of sampling or preservational biases in all subintervals.

Since our CONOP.SAGA composite is composed of 11,326 discrete temporal levels, this provided us with 11,326 counting points. We first calculate the total diversity at each counting point, which is equal to n_t, the total number of taxa crossing the top boundary (*26*). Diversity at each counting point was divided by the section number at each point to get the per-section diversity (*23*). Similar to the standard data smoothing technique – Moving Average, we created a 10-Myr time bin on each counting point (fig. S7) in order to calculate the average total diversity and per-section diversity of each bin. Diversity at each counting point was further standardized or smoothed using the average total diversity and per-section diversity. This time bin was then slide to the next counting point and the calculations repeated. These standardizations have the effect of smoothing the diversity curve, and even reduced the peak located before the end-Permian mass extinction.

The equations are as follow:

At time t, we have data $\mathrm{N}_{\mathrm{Ft}}^{t}$, $\mathrm{N}_{\mathrm{bt}}^{t}$, and $\mathrm{N}_{\mathrm{t}}^{t} = \mathrm{N}_{\mathrm{Ft}}^{t} + \mathrm{N}_{\mathrm{bt}}^{t}$ (*26*).
The amount of sections at time t is $n_{sec}(t)$.
The amount of chosen time points is n_t.
The adjusted total diversity at time t is

$$\hat{d}_{tot}(t) = \mathrm{N}_{\mathrm{Ft}}^{t} + \mathrm{N}_{\mathrm{bt}}^{t} = \mathrm{N}_{\mathrm{t}}^{t}$$

The per-section diversity at time t is

$$d_{per-sec}(t) = \frac{\hat{d}_{tot}(t)}{n_{sec}(t)}$$

The standardized per-section diversity (modified from the rescaled per-section diversity of Sadler et al., *(14)*) at time t is

$$\hat{d}_{per-sec}(t) = d_{per-sec}(t) \cdot \frac{\bar{d}_{tot}}{\bar{d}_{per-sec}}$$

where $\bar{d}_{tot}$ is the mean of $\hat{d}_{tot}(t)$ along time (i.e., 10-Myr time bin herein),

$$\bar{d}_{tot} = \frac{\sum_{i=1}^{n_t} \hat{d}_{tot}(t_i)}{n_t}$$

and $\bar{d}_{per-sec}$ is the mean of $d_{per-sec}(t)$ along time (i.e., 10-Myr time bin herein),

$$\bar{d}_{per-sec} = \frac{\sum_{i=1}^{n_t} d_{per-sec}(t_i)}{n_t}$$

It is worth noting that our diversity curves do not attempt to correct for the missing species which did not leave a fossil record. Although CONOP can largely eliminate the incompleteness of fossil records through adjustments of fossil extensions based on different existing fossil sequences from different sections, bias may still exist due to incomplete fossil preservation. We have not attempted to statistically adjust first and last appearances to account for preservational or sampling biases at range endpoints.

In future we intend to undertake a more complete analysis of bias in our diversity summary via application of more sophisticated standardization procedures (e.g., Shareholder Quorum Subsampling (*68*), True Richness estimated using the Poisson Sampling model (*69*)).

As shown in Figures 1A and S6, both species and genus diversities increased by greater than a factor of 3 from the Late Cambrian to Middle Ordovician Darriwilian Age, and then remained near ~500 species for 11.89 Myr until the Sandbian (early Late Ordovician). The pattern from Late Ordovician to Early Silurian recorded by our data differs from many previous studies (Fig. 2A; *4, 10*).

Based on our study, a protracted Late Ordovician diversity decline occurred from the Sandbian, 14 Myr before the Ordovician–Silurian boundary (455.44 Ma) and reached a diversity minimum at 443.9 Ma in the Hirnantian (Fig. 1A). This may

represent a regional event in South China, possibly due to a shift from a shallow carbonate-dominated facies in the Sandbian to anoxic dominated facies in the Katian. All major fossils groups including trilobites, graptolites and conodonts started to decline from the Sandbian (Fig. 1B and fig. S10).

The protracted decline of diversity from Middle to Late Devonian was likely caused by a series of events during the Middle and Late Devonian (e.g., Chotec, Kacak, Thaganic, Frasne, Lower and Upper Kellwasser events) which progressively reduced species diversity. Our results indicate the Frasnian–Famennian extinction was a more prolonged diversity crisis than that previously indicated, at least in China.

Species diversity increased by a factor of ~3.5 from the late Visean to the late Asselian (294.80 Ma) with a distinct decline in the Moscovian and Kasimovian. This may represent another unrecognized biological event. The Lopingian diversity peak was not recognized by Alroy et al. (*4*), but shows up clearly in our data as increased diversities of brachiopods, bivalves and cephalopods.

The ~780 kyr decline prior to the sudden drop at the end of the Permian may reflect an actual drop in diversity or incompleteness of the fossil record in different sections. If end-Permian diversity declined rapidly within the last 780 kyr of the Lopingian, this may reflect environmental deterioration triggered by intensive volcanism (e.g., Siberian Traps; *70*) followed by a sudden ecosystem collapse at 251.95 Ma (cf. *71*). However, we cannot exclude the possibility that this apparent progressive decline may be due to the incompleteness of fossil records in different sections. Our fossil range data show that different sections have distinct patterns of disappearance and appearance of new clades, likely reflecting different environmental settings. Although our CONOP.SAGA algorithms search to find the best fit to use in constructing the composite reference section in order to compensate for the incompleteness of the fossil record, it cannot eliminate this problem entirely.

5. Estimation of the effect of temporal resolution on paleobiodiversity analysis

The high-resolution composite sequence produced by our study also provides an opportunity to estimate the effect of temporal resolution on paleobiodiversity analysis. To effect this comparison, we divided the 300 Myr duration (540 to 240 Ma) into 30 10-Myr time bins. Then all the first and last appearance events were allocated to these time bins and the number of species in each bin totaled to generate a 10-Myr species diversity curve (Fig. 3). By performing similar calculations using 5-Myr, 2-Myr, 1-Myr, 0.5-Myr, 0.2-Myr and 0.1-Myr time bins, we produced a series of binned, temporally even diversity curves at different temporal resolutions (Fig. 3). As shown in fig. S11, the time bins employed by Alroy et al. (*4*) exhibited uneven durations. We divide our high-resolution composite section into the same time bins used by Alroy et al. (*10*), so that we could compare our unbinned paleobiodiversity data to the pattern that would be obtained if these same data were passed through the Alroy et al. (*21*) uneven temporal division filter (Fig. 3, dashed blue line).

6. Correlation analysis of the species diversity and other environmental proxies

Simple scatter plots used to show the distribution of the species diversity and other environmental proxies including long-term P_{CO_2} with data from Visean (*58*), $^{87}Sr/^{86}Sr$ with data from McArthur et al. (*60*), $\delta^{18}O$ with data from Veizer and Prokoph (*62*), $\delta^{13}C$ with data from Saltzman and Thomas (*53*), continental fragmentation index with data from Zaffos et al. (*10*). In addition to the scatterplots which give an intuitive view of trends in these curves, their correlations were analyzed considering both Pearson's and Yule's views on correlation.

These data depict similar secular trends between the species diversity and the long-term P_{CO_2} as shown in Fig. 5A. Both curves show general decreasing trends from 253 Ma to 343 Ma and increasing trends from 343 to 419 Ma (fig. 5B). The simple Pearson Product-Moment correlation coefficient between these two curves, and the results as shown in Fig. 5B, indicate strong positive correlations for the interval from 343 to 253 Ma ($R^2 = 0.70$, *t*-value = 13.2, $n = 77$) and for the interval from 419 to 343 ($R^2 = 0.52$, *t*-value = 9.72, $n = 90$). For both intervals, Students *t*-values were calculated using the following equation: $R*sqrt((n-2)/(1-R^2))$.

However, considering that the strong trends present of these curves may have effected these results, we detrended both by subtracting from each point the value of the preceding point: $y'(t) = y(t) – y(t-1)$ and $x'(t) = x(t) – x(t-1)$ according to the first difference method (*72*). The correlation analysis was then applied to these two detrended curves. The results are shown in Fig. 5C-D and figs. S13A-B. In addition to straight correlation cross correlation between these two detrended curves with lagged times was implemented. The results obtained with a lagged time 4 Myr is given in fig. S13B. All results shown in Fig. 5 and fig. S13 suggest that, once the effect of trend similarity has been removed, there is no significant correlation between the changes in species diversity (Myr to Myr) and changes in P_{CO_2} (Myr to Myr). Our analysis reveals that similar secular trends do exist between curves of P_{CO_2} and the diversity which implies that these two curves may be influenced by a largely common set of driving factors. However, this apparent similarity reflects the similarity in their (lagged) trends, not their fine structure. Our results support Yule's cautionary principle that time series curves depicting similar secular trends might not be necessarily correlated or causally associated, though further research into the association between these time series — especially in their dates associated with the P_{CO_2} curve, needs to be undertaken.

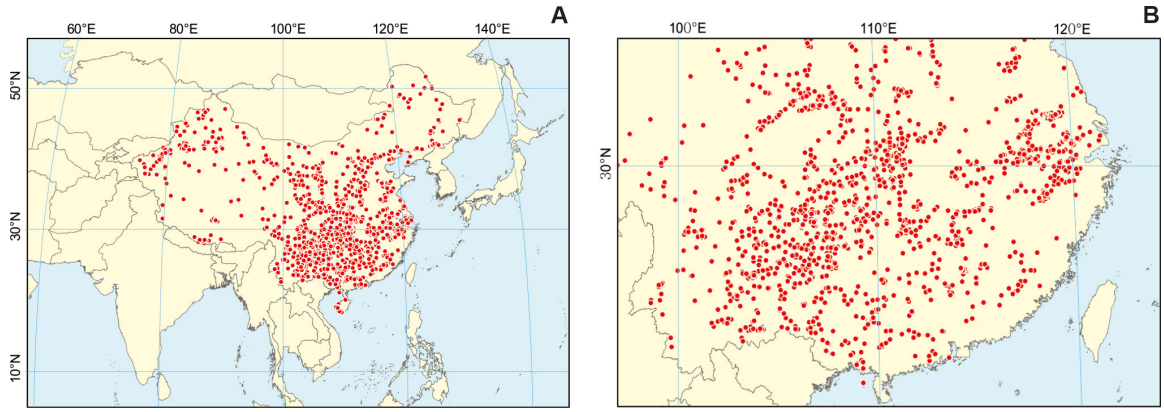

Fig. S1. Distribution of Paleozoic sections in China used in the present study. (A) Distribution of studied Chinese sections on modern geographic map. (B) A detailed map of South China showing the sampling intensity of our database.

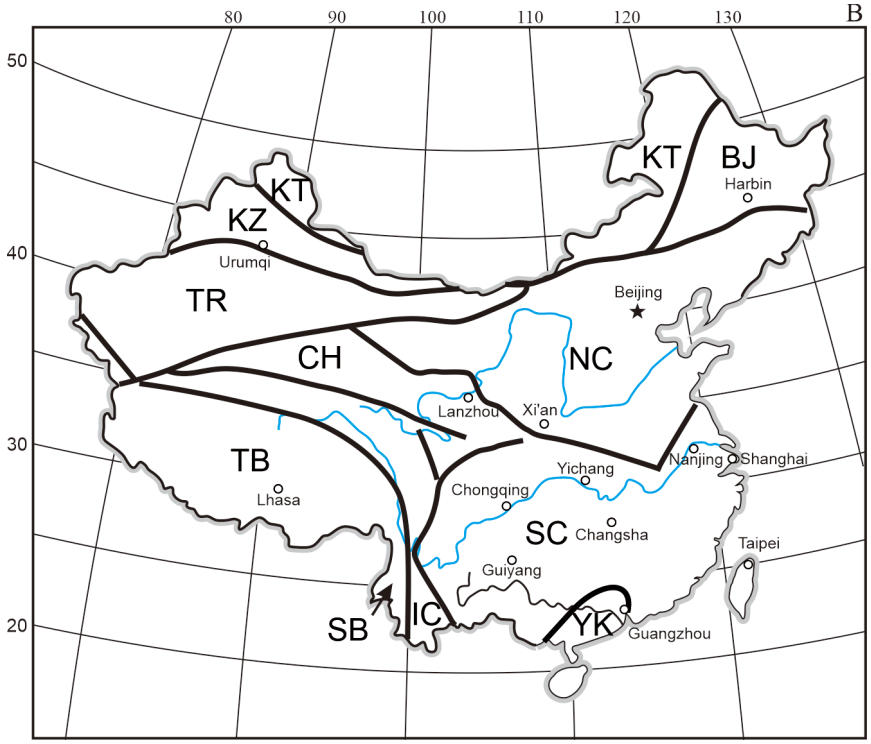

Fig. S2. Geological map showing the main Chinese paleoplates (after *(18)*). The map is mainly for the early Paleozoic. BJ, Bureya–Jiamusi; CH, Chaidamu; IC, Indochina; KT, Khingan–Tuva; KZ, Kazakhstan; NC, North China; SB, Sibumasu; SC, South China; TB, Tibet (Xizang); TR, Tarim; YK, Yunkai.

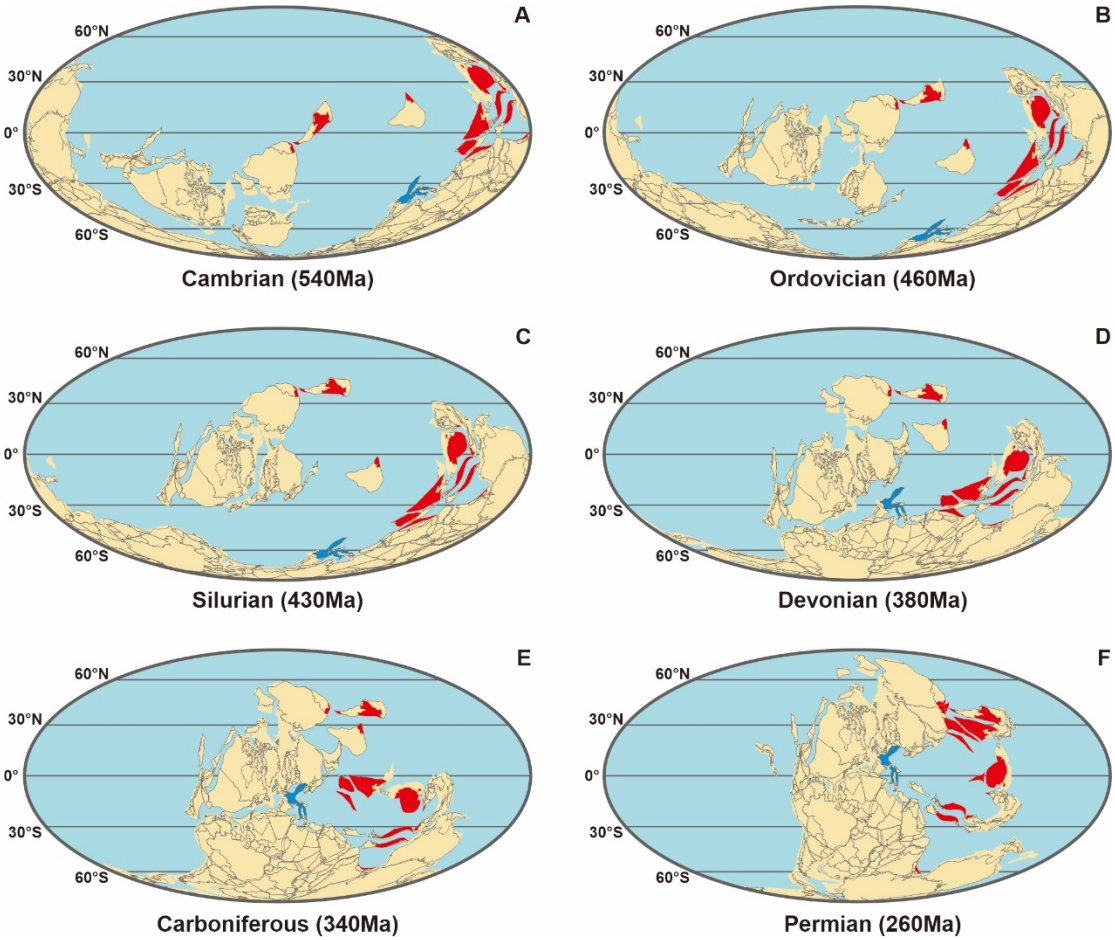

Fig. S3. Paleogeographic maps showing the paleopositions of major blocks in China during the Paleozoic (based on *73*). Red areas represent the paleopositions of Chinese blocks. Blue areas indicate the paleopositions of European blocks included in the present study.

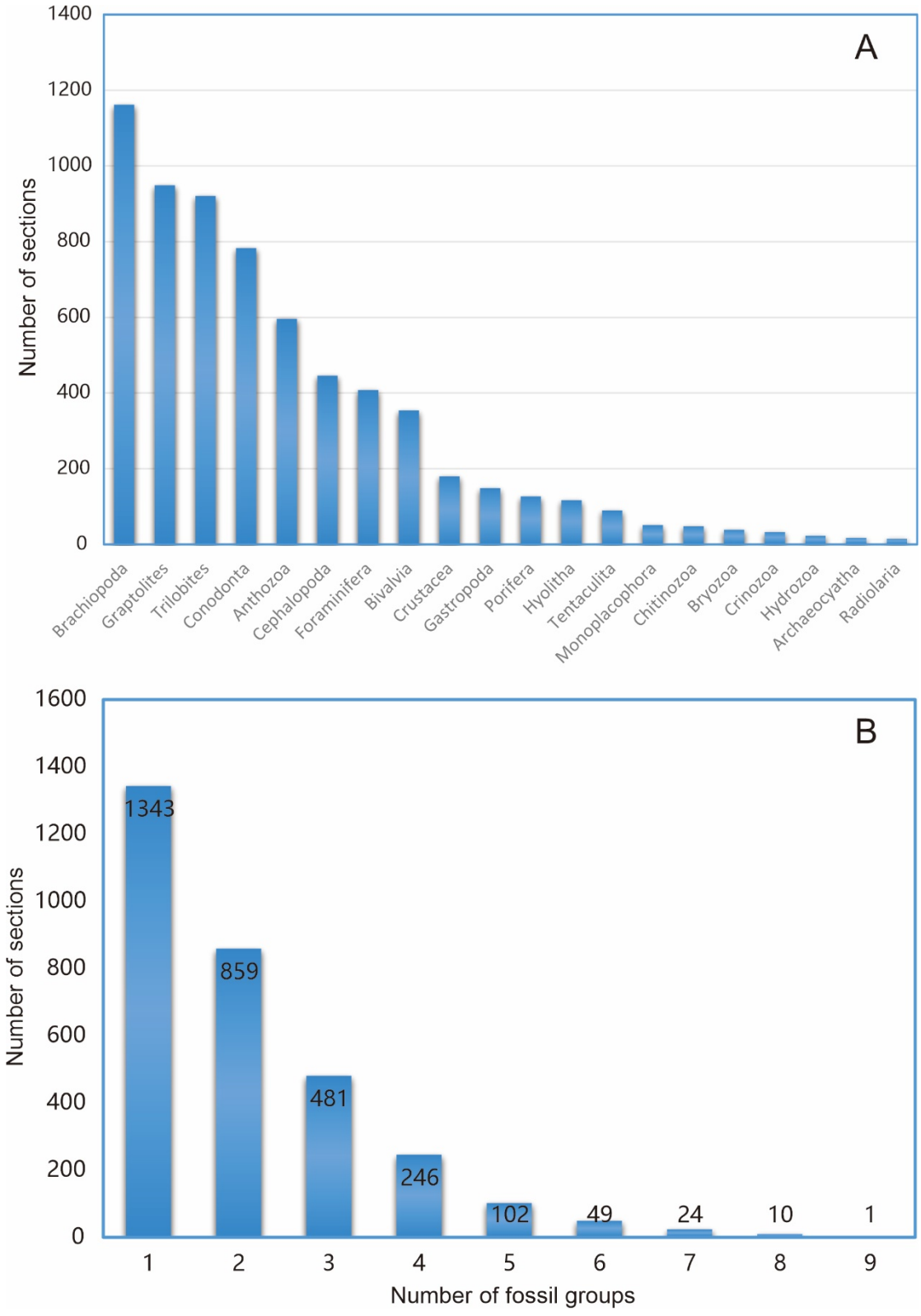

Fig. S4. Distribution of the fossil groups in the studied sections. (A) Distribution of each fossil group in the studied sections. (B) Distribution of fossil groups counts in the studied sections.

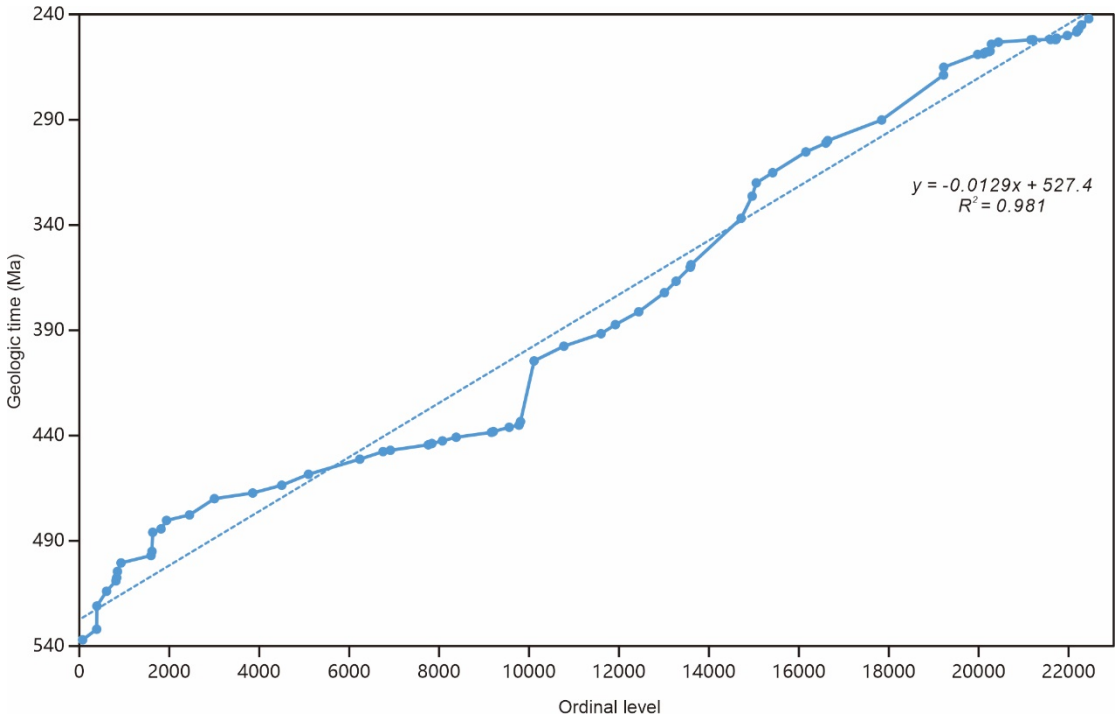

Fig. S5. Age-level model for the present study. Dots represent the geologic ages corresponding to 70 zonal fossils.

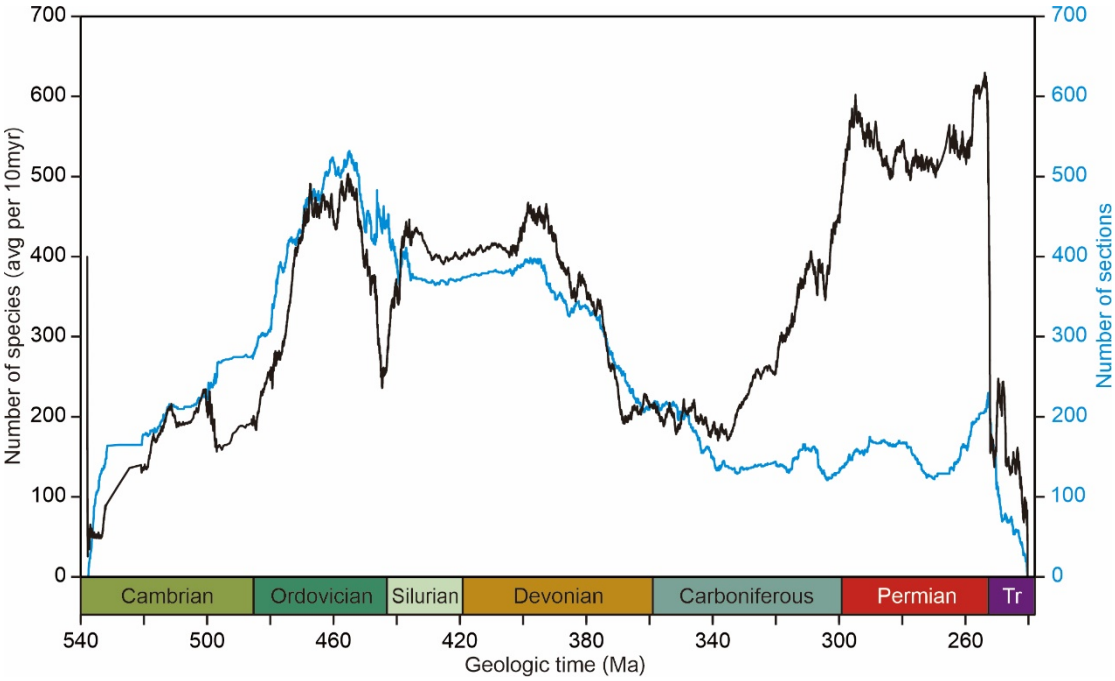

Fig. S6. Standardized species diversity curve (black) and the curve of section numbers (blue). By using the sliding bin calculation technique, the species diversity was standardized using the average diversity and section number in each 10-Myr bin.

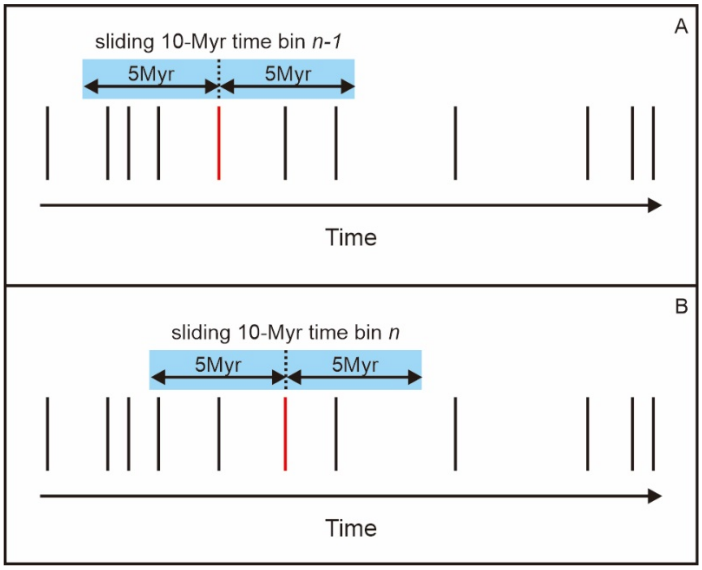

Fig. S7. Principle of counting the average number of sections inside a sliding 10-Myr time bin which is centered on each counting point. The counting point in red represents a first or last appearance event in the composite. (A) If a 5-Myr time bin is placed before the counting point and another behind it, then a bin of 10-Myr duration will be created within which the average number of sections of the 10-Myr interval can be counted. (B) Movement to the next counting point (next first or last appearance event) in the composite section where the calculation is repeated. Thus, a 10-Myr moving-average curve was produced to removing possible biases.

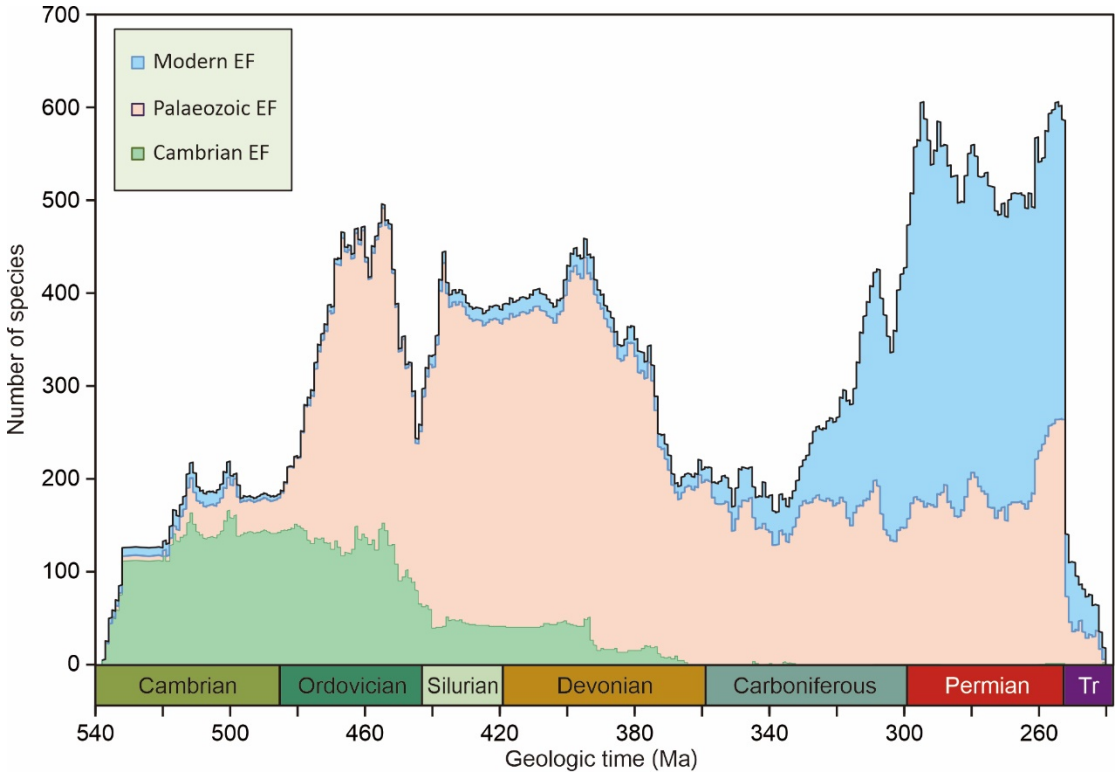

Fig. S8. Species-level diversity curves for the three marine evolutionary faunas. EF-evolutionary fauna

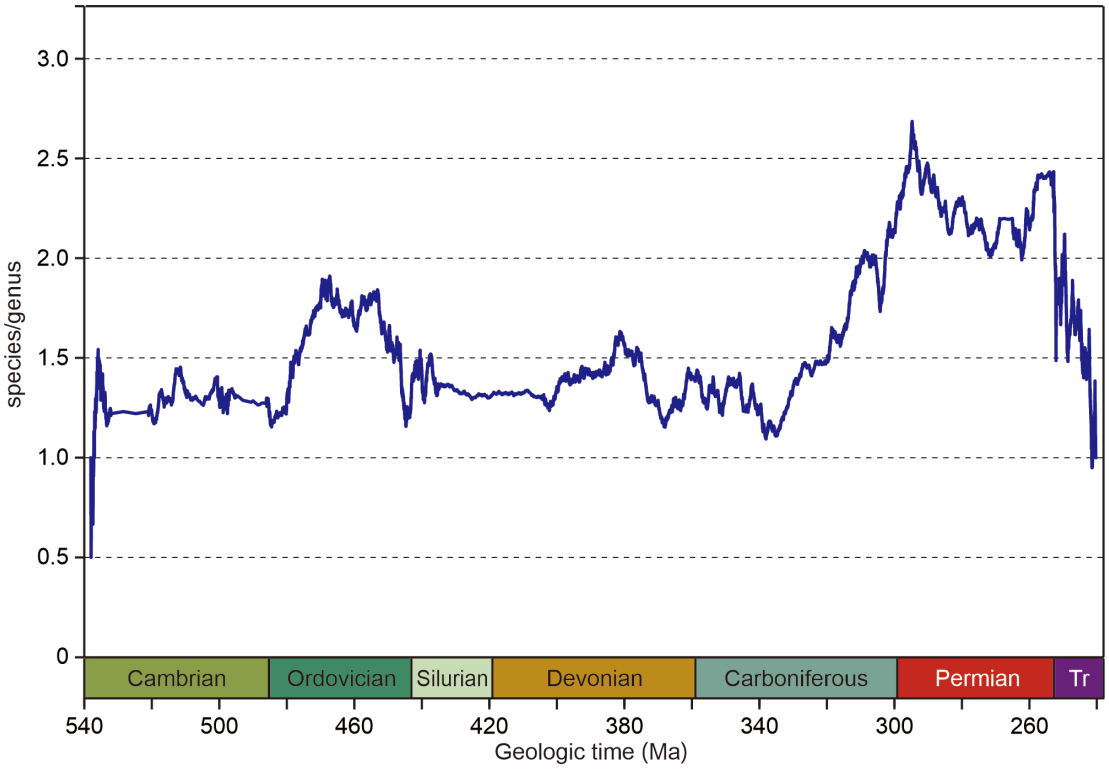

Fig. S9. Species/genus ratio trend through the Paleozoic. As shown in this figure, the GOBE and the Carboniferous–Permian Biodiversification Event were associated with global cooling (*42, 74*). One plausible explanation is that these changes reflect a sharpening of the latitudinal diversity gradient. Similar patterns are found, for example, in the species/genus ratio for marine benthic molluscs along the northeastern Pacific coast. However, some other factors (e.g., species competition, changing taxonomic composition, endemism, sampling effect) may play roles in the changes of species/genus ratio (*75, 76*).

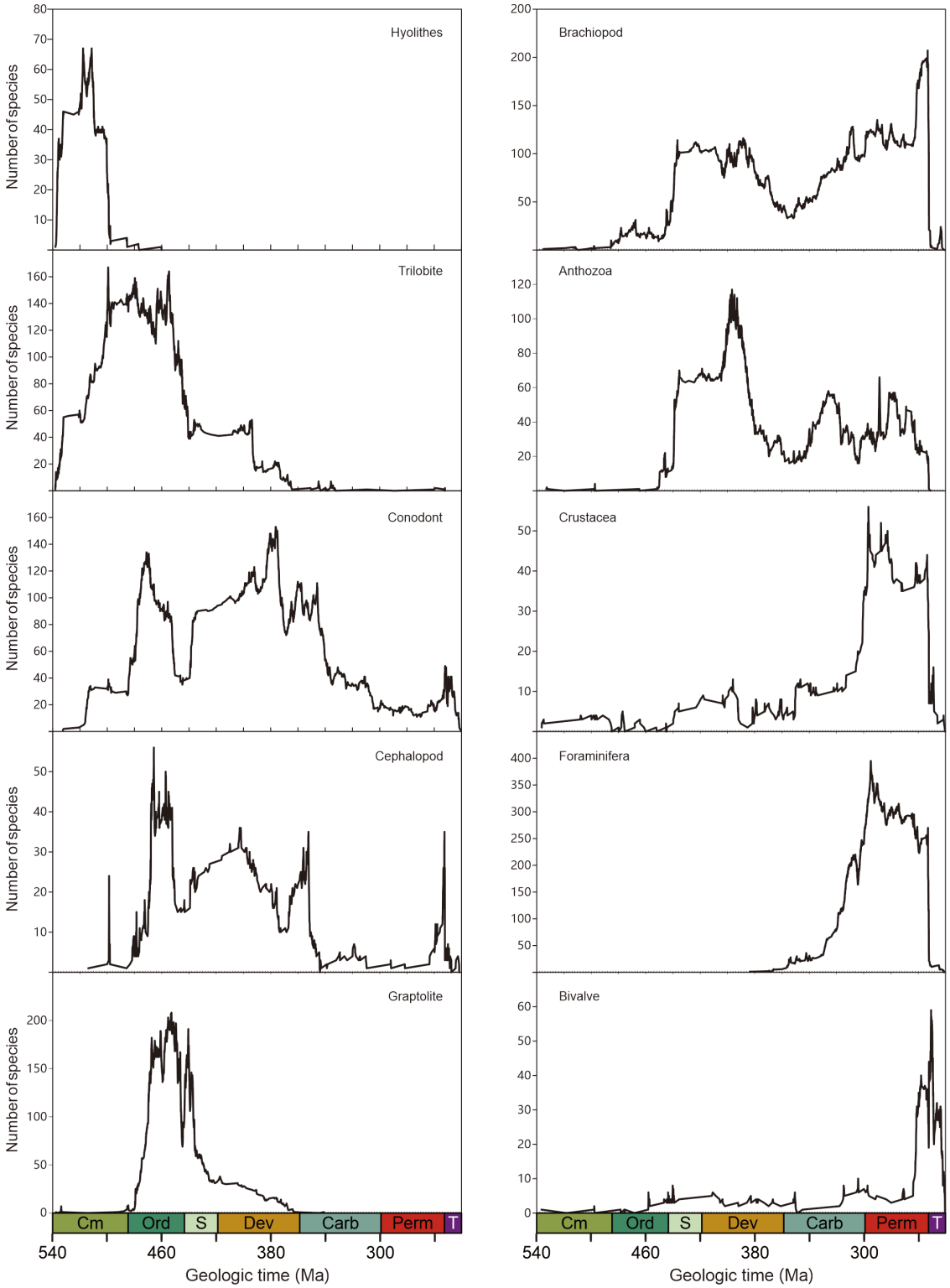

Fig. S10. Paleozoic species diversity curves of ten major fossil groups.

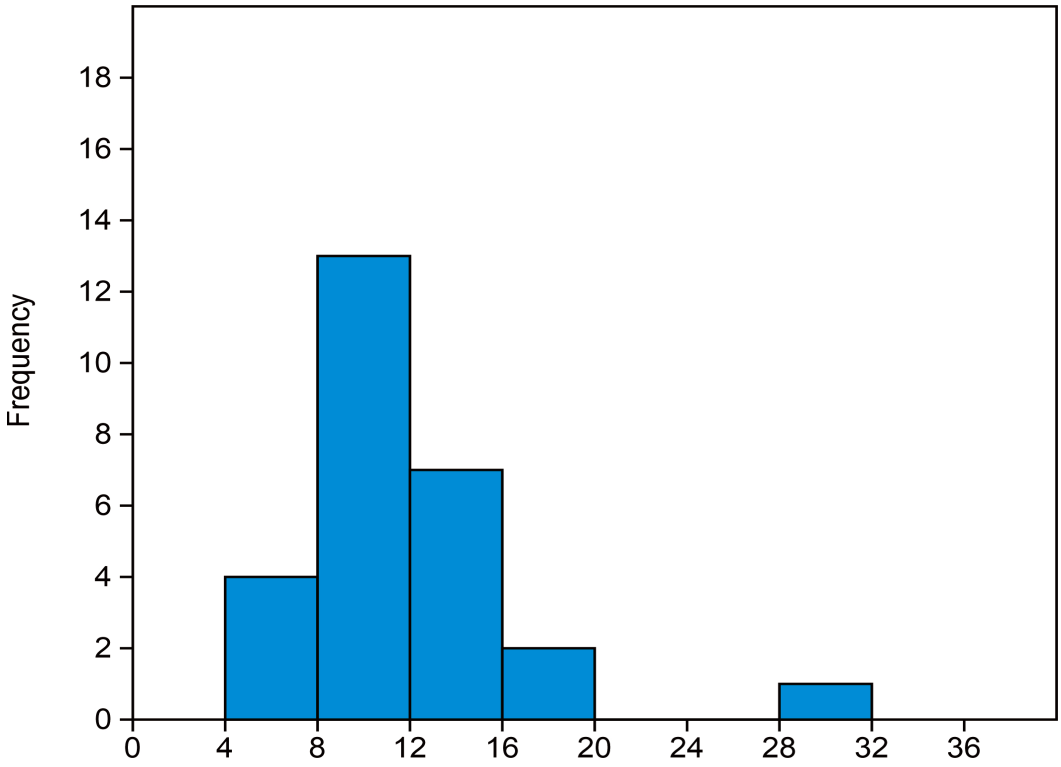

Fig. S11. Histogram of time-bin durations used by Alroy et al. (*4*).

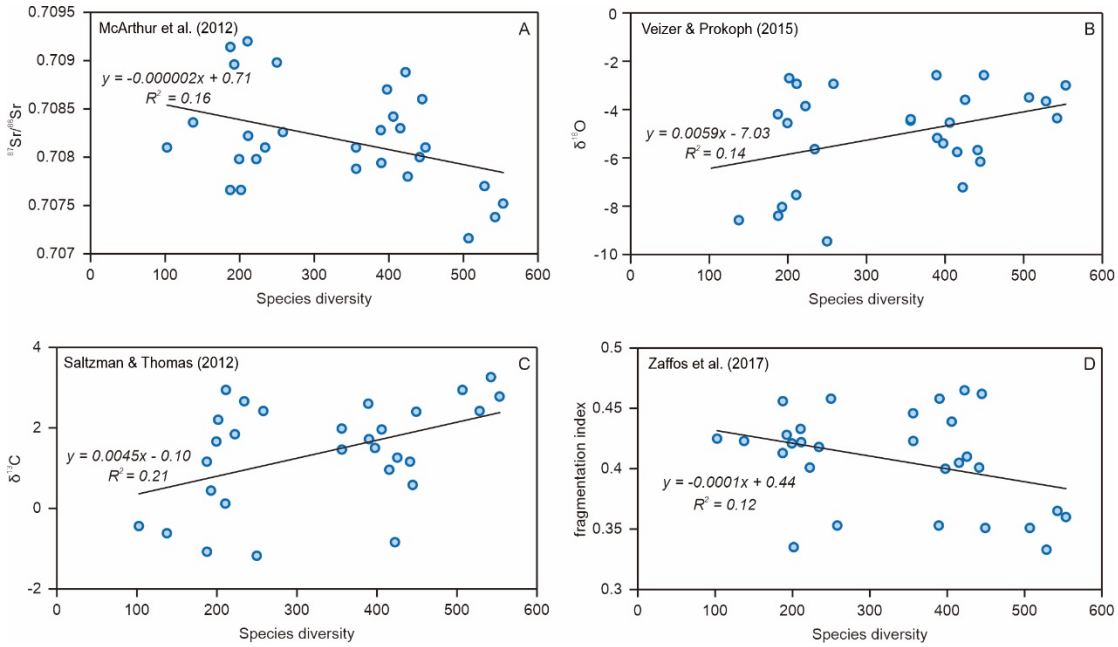

Fig. S12. Plots showing associations of the species diversity and four other environmental proxies. A, $Sr^{87}/^{86}Sr$, data from McArthur et al. (*60*); B, $\delta^{18}O$, data from Veizer and Prokoph (*62*); C, $\delta^{13}C$, data from Saltzman and Thomas (*53*); D, continental fragmentation index, data from Zaffos et al. (*10*). Data do not show strong correlation.

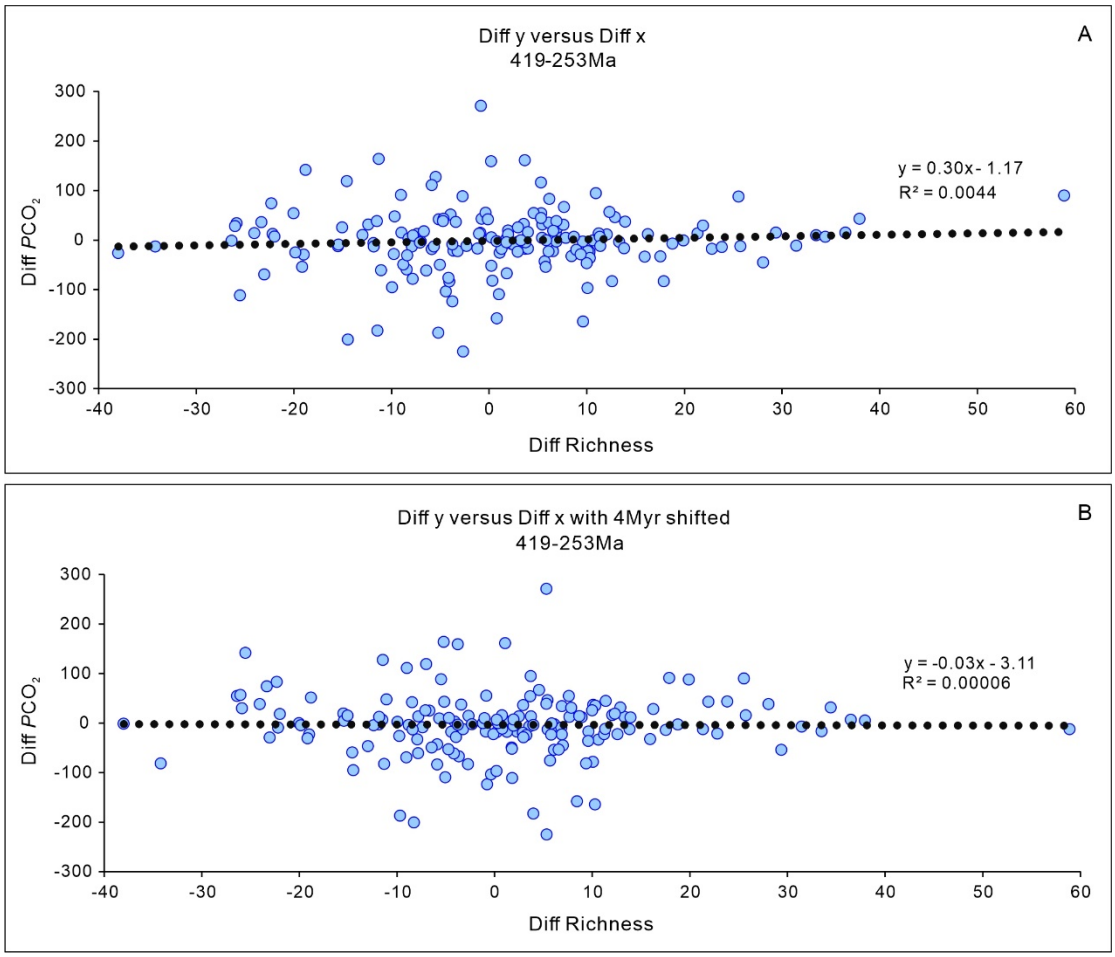

Fig. S13. Analysis of associations of the species diversity and PCO_2. A, correlation between changes in diversity and changes in PCO_2; B, cross correlation between the two curves of changes in diversity and in PCO_2 with lagged time 4 Myr. Several lagged times were implemented and none of them show correlation.

Table S1. Index fossils used for the construction of the composite sequence.

	Species name
1	*Paragondolella inclinata*
2	*Nicoraella kockeli*
3	*Chiosella timorensis*
4	*Neospathodus triangularis*
5	*Icriospathodus collinsoni*
6	*Triassospathodus homeri*
7	*Novispathodus pingdingshanensis*
8	*Neospathodus waageni*
9	*Neospathodus dieneri*
10	*Sweetospathodus kummeli*
11	*Clarkina krystyni*
12	*Clarkina planata*
13	*Isarcicella isarcica*
14	*Isarcicella staeschei*
15	*Hindeodus parvus*
16	*Clarkina meishanensis*
17	*Clarkina yini*
18	*Clarkina changxingensis*
19	*Clarkina wangi*
20	*Clarkina orientalis*
21	*Clarkina transcaucasica*
22	*Clarkina guangyuanensis*
23	*Clarkina leveni*
24	*Clarkina asymmetrica*
25	*Clarkina dukouensis*
26	*Clarkina postbitteri postbitteri*
27	*Clarkina postbitteri hongshuiensis*

	Species name
28	*Jinogondolella granti*
29	*Jinogondolella xuanhanensis*
30	*Jinogondolella prexuanhanensis*
31	*Jinogondolella altudaensis*
32	*Jinogondolella shannoni*
33	*Jinogondolella postserrata*
34	*Jinogondolella aserrata*
35	*Sweetognathus guizhouensis*
36	*Neostreptognathodus prayi*
37	*Neostreptognathodus pequopensis*
38	*Sweetognathus whitei*
39	*Sweetognathus merrilli*
40	*Streptognathodus wabaunsensis*
41	*Streptognathodus simplex*
42	*Streptognathodus cancellosus*
43	*Montiparus paramontiparus*
44	*Fusulinella bocki*
45	*Fusulinella colaniae*
46	*Profusulinella parva*
47	*Pseudostaffella praegorskyi*
48	*Idiognathodus sinuatus*
49	*Eostaffellina protvae*
50	*Eostaffella ikensis*
51	*Gnathodus bilineatus*
52	*Polygnathus communis*
53	*Siphonodella isosticha*
54	*Siphonodella sandbergi*

	Species name
55	*Siphonodella duplicata*
56	*Siphonodella sulcata*
57	*Siphonodella praesulcata*
58	*Palmatolepis gracilis expansa*
59	*Palmatolepis marginifera*
60	*Palmatolepis crepida*
61	*Palmatolepis triangularis*
62	*Palmatolepis hassi*
63	*Palmatolepis punctata*
64	*Palmatolepis transitans*
65	*Schmidtognathus hermanni*
66	*Viriatellina minuta*
67	*Polygnathus varcus*
68	*Nowakia otomari*
69	*Tortodus kockelianus kockelianus*
70	*Polygnathus costatus costatus*
71	*Polygnathus costatus partitus*
72	*Polygnathus costatus patulus*
73	*Polygnathus serotinus*
74	*Nowakia cancellata*
75	*Nowakia elegans*
76	*Nowakia barrandei*
77	*Nowakia praecursor*
78	*Nowakia zlichovensis*
79	*Nowakia acuaria*
80	*Paranowakia intermedia*
81	*Monograptus praehercynicus*

	Species name
82	*Cyrtograptus murchisoni*
83	*Pterospathodus amorphognathoides*
84	*Cyrtograptus lapworthi*
85	*Oktavites spiralis*
86	*Monoclimacis griestoniensis*
87	*Pterospathodus eopennatus*
88	*Spirograptus turriculatus*
89	*Spirograptus guerichi*
90	*Demirastrites convolutus*
91	*Demirastrites triangulatus*
92	*Atavograptus atavus*
93	*Coronograptus cyphus*
94	*Cystograptus vesiculosus*
95	*Parakidograptus acuminatus*
96	*Akidograptus ascensus*
97	*Metabolograptus persculptus*
98	*Metabolograptus extraordinarius*
99	*Tangyagraptus typicus*
100	*Paraorthograptus pacificus*
101	*Dicellograptus complexus*
102	*Diplacanthograptus spiniferus*
103	*Diplacanthograptus caudatus*
104	*Baltoniodus alobatus*
105	*Orthograptus calcaratus*
106	*Climacograptus bicornis*
107	*Nemagraptus gracilis*
108	*Pygodus anserinus*

	Species name
109	*Pygodus serra*
110	*Didymograptus murchisoni*
111	*Pterograptus elegans*
112	*Eoplacognathus suecicus*
113	*Didymograptus artus*
114	*Undulograptus austrodentatus*
115	*Paroistodus originalis*
116	*Baltoniodus navis*
117	*Baltoniodus triangularis*
118	*Azygograptus suecicus*
119	*Didymograptus deflexus*
120	*Oepikodus evae*
121	*Tetragraptus approximatus*
122	*Paltodus deltifer*
123	*Cordylodus angulatus*
124	*Hysterolenus asiaticus*
125	*Leiostegium (leiostegium) constrictum*
126	*Probilacunaspis nasalis*
127	*Corynexochus plumula*
128	*Glyptagnostus reticulatus*
129	*Glyptagnostus stolidotus*
130	*Lejopyge laevigata*
131	*Lejopyge armata*
132	*Goniagnostus nathorsti*
133	*Ptychagnostus punctuosus*
134	*Ptychagnostus atavus*
135	*Peronopsis taijiangensis*

	Species name
136	*Oryctocephalus indicus*
137	*Arthricocephalus chauveaui*
138	*Tsunyidiscus niutitangensis*
139	*Paragloborilus subglobosus*
140	*Anabarites trisulcatus*

Table S2. Interpolated geochronologic ages for all fossil zones used in the calibration of the composite sequence.

	Biozone	Age
1	*Anabarites trisulcatus*	537Ma
2	*Paragloborilus subglobosus*	532Ma
3	*Tsunyidiscus niutitangensis*	521Ma
4	*Arthricocephalus chauveaui*	514Ma
5	*Oryctocephalus indicus*	509Ma
6	*Peronopsis taijiangensis*	507.5Ma
7	*Ptychagnostus atavus*	504.5Ma
8	*Lejopyge laevigata*	500.5Ma
9	*Glyptagnostus reticulatus*	497Ma
10	*Corynexochus plumula*	495Ma
11	*Hysterolenus asiaticus*	486Ma
12	*Cordylodus angulatus*	484.3Ma
13	*Paltodus deltifer*	480.3Ma
14	*Tetragraptus approximatus*	477.7Ma
15	*Baltoniodus navis*	470Ma
16	*Undulograptus austrodentatus*	467.3Ma
17	*Didymograptus murchisoni*	463.6Ma
18	*Nemagraptus gracilis*	458.4Ma
19	*Diplacanthograptus spiniferus*	451.2Ma
20	*Dicellograptus complexus*	447.6Ma
21	*Paraorthograptus pacificus*	447Ma
22	*Metabolograptus persculptus*	444.4Ma
23	*Akidograptus ascensus*	443.8Ma
24	*Cystograptus vesiculosus*	442.5Ma
25	*Demirastrites triangulatus*	440.8Ma
26	*Spirograptus guerichi*	438.5Ma

	Biozone	Age
27	*Spirograptus turriculatus*	438.1Ma
28	*Oktavites spiralis*	436.1Ma
29	*Cyrtograptus lapworthi*	435.1Ma
30	*Cyrtograptus murchisoni*	433.4Ma
31	*Polygnathus gronbergi*	404.6Ma
32	*Polygnathus serotinus*	397.6Ma
33	*Polygnathus costatus costatus*	391.6Ma
34	*Polygnathus varcus*	387.3Ma
35	*Palmatolepis transitans*	381.2Ma
36	*Palmatolepis triangularis*	372.2Ma
37	*Palmatolepis marginifera*	366.7Ma
38	*Siphonodella praesulcata*	360Ma
39	*Siphonodella sulcata*	358.9Ma
40	*Gnathodus bilineatus*	336.8Ma
41	*Eostaffellina protvae*	326.3Ma
42	*Pseudostaffella praegorskyi*	320Ma
43	*Profusulinella aljutovica*	315.2Ma
44	*Streptognathodus cancellosus*	305.3Ma
45	*Streptognathodus simplex*	301.1Ma
46	*Streptognathodus wabaunsensis*	299.9Ma
47	*Sweetognathus whitei*	290.1Ma
48	*Jinogondolella aserrata*	268.8Ma
49	*Jinogondolella postserrata*	265.1Ma
50	*Clarkina postbitteri postbitteri*	259Ma
51	*Clarkina dukouensis*	258.7Ma
52	*Clarkina asymmetrica*	258.4Ma
53	*Clarkina leveni*	258.1Ma

	Biozone	Age
54	*Clarkina guangyuanensis*	257.9Ma
55	*Clarkina transcaucasica*	257.6Ma
56	*Clarkina orientalis*	257.4Ma
57	*Clarkina wangi*	254.14Ma
58	*Clarkina changxingensis*	253.123Ma
59	*Clarkina yini*	252.046Ma
60	*Clarkina meishanensis*	251.952Ma
61	*Hindeodus parvus*	251.902Ma
62	*Isarcicella staeschei*	251.889Ma
63	*Isarcicella isarcica*	251.873Ma
64	*Clarkina krystyni*	251.3Ma
65	*Neospathodus waageni*	250Ma
66	*Icriospathodus collinsoni*	248.27Ma
67	*Neospathodus triangularis*	247.6Ma
68	*Chiosella timorensis*	247.1Ma
69	*Nicoraella kockeli*	245Ma
70	*Paragondolella inclinata*	242Ma

Table S3. Mean temporal resolution of each Paleozoic system.

	Base level	Top level	Base age (Ma)	Top age (Ma)	Mean resolution (kyr)
Cambrian	1	953	539.0673	477.7	64.46
Ordovician	953	4066	477.7	443.8	10.89
Silurian–Devonian	4066	6914	443.8	358.9	29.81
Carboniferous	6914	8580	358.9	298.9	36.01
Permian	8580	10764	298.9	252.2	21.38

References and Notes

1. J. J. Sepkoski Jr., *A Compendium of Fossil Marine Animal Families* (Milwaukee Public Museum, ed. 2, 1992)

2. J. J. Sepkoski Jr., *A Compendium of Fossil Marine Animal Genera* (Paleontological Research Institution, 2002).

3. J. Alroy, C. R. Marshall, R. K. Bambach, K. Bezusko, M. Foote, F. T. Fursich, T. A. Hansen, S. M. Holland, L. C. Ivany, D. Jablonski, D. K. Jacobs, D. C. Jones, M. A. Kosnik, S. Lidgard, S. Low, A. I. Miller, P. M. Novack-Gottshall, T. D. Olszewski, M. E. Patzkowsky, D. M. Raup, K. Roy, J. J. Sepkoski Jr., M. G. Sommers, P. J. Wagner, A. Webber, Effects of sampling standardization on estimates of Phanerozoic marine diversification. *Proc. Natl. Acad. Sci. U.S.A.* **98**, 6261–6266 (2001). doi:10.1073/pnas.111144698 Medline

4. J. Alroy, M. Aberhan, D. J. Bottjer, M. Foote, F. T. Fürsich, P. J. Harries, A. J. W. Hendy, S. M. Holland, L. C. Ivany, W. Kiessling, M. A. Kosnik, C. R. Marshall, A. J. McGowan, A. I. Miller, T. D. Olszewski, M. E. Patzkowsky, S. E. Peters, L. Villier, P. J. Wagner, N. Bonuso, P. S. Borkow, B. Brenneis, M. E. Clapham, L. M. Fall, C. A. Ferguson, V. L. Hanson, A. Z. Krug, K. M. Layou, E. H. Leckey, S. Nürnberg, C. M. Powers, J. A. Sessa, C. Simpson, A. Tomasovych, C. C. Visaggi, Phanerozoic trends in the global diversity of marine invertebrates. *Science* **321**, 97–100 (2008). doi:10.1126/science.1156963 Medline

5. R. K. Bambach, Phanerozoic biodiversity mass extinctions. *Annu. Rev. Earth Planet. Sci.* **34**, 127–155 (2006). doi:10.1146/annurev.earth.33.092203.122654

6. C. M. O. Rasmussen, B. Kröger, M. L. Nielsen, J. Colmenar, Cascading trend of Early Paleozoic marine radiations paused by Late Ordovician extinctions. *Proc. Natl. Acad. Sci. U.S.A.* **116**, 7207–7213 (2019). doi:10.1073/pnas.1821123116 Medline

7. J. Alroy, Colloquium paper: Dynamics of origination and extinction in the marine fossil record. *Proc. Natl. Acad. Sci. U.S.A.* **105**, 11536–11542 (2008). doi:10.1073/pnas.0802597105 Medline

8. B. Hannisdal, S. E. Peters, Phanerozoic Earth system evolution and marine biodiversity. *Science* **334**, 1121–1124 (2011). doi:10.1126/science.1210695 Medline

9. S. E. Peters, M. Foote, Biodiversity in the Phanerozoic: A reinterpretation. *Paleobiology* **27**, 583–601 (2001). doi:10.1666/0094-8373(2001)027<0583:BITPAR>2.0.CO;2

10. A. Zaffos, S. Finnegan, S. E. Peters, Plate tectonic regulation of global marine animal diversity. *Proc. Natl. Acad. Sci. U.S.A.* **114**, 5653–5658 (2017). doi:10.1073/pnas.1702297114 Medline

11. M. J. Benton, Ed., *The Fossil Record 2* (Chapman & Hall, 1993).

12. J. Alroy, Fair sampling of taxonomic richness and unbiased estimation of origination and extinction rates. *Paleontol. Soc. Pap.* **16**, 55–80 (2010). doi:10.1017/S1089332600001819

13. O. H. Walliser, Ed., *Global Events and Event Stratigraphy in the Phanerozoic* (Springer, 1996).

14. P. M. Sadler, R. A. Cooper, M. J. Melchin, High-resolution, early Paleozoic (Ordovician-Silurian) time scales. *Geol. Soc. Am. Bull.* **121**, 887–906 (2009). doi:10.1130/B26357.1

15. J. X. Fan, Q. Chen, X. D. Hou, A. I. Miller, M. J. Melchin, S. Z. Shen, S. Y. Wu, D. Goldman, C. E. Mitchell, Q. Yang, Y. D. Zhang, R. B. Zhan, J. Wang, Q. Leng, H. Zhang, L. N. Zhang, Geobiodiversity Database: A comprehensive section-based integration of stratigraphic and paleontological data. *Newsl. Stratigr.* **46**, 111–136 (2013). doi:10.1127/0078-0421/2013/0033

16. Materials and methods are available as supplementary materials.

17. A. J. Boucot, X. Chen, C. R. Scotese, R. J. Morley, "Phanerozoic paleoclimate: An atlas of lithologic indicators of climate" in G. J. Nichols, B. Ricketts, Eds., *SEPM Concepts in Sedimentology and Paleontology* (SEPM, Tulsa, 2013), vol. 11, pp. 478.

18. J. Y. Rong, J. X. Fan, A. I. Miller, G. X. Li, Dynamic patterns of latest Proterozoic-Palaeozoic-early Mesozoic marine biodiversity in South China. *Geol. J.* **42**, 431–454 (2007). doi:10.1002/gj.1073

19. P. M. Sadler, R. A. Cooper, "Best-fit intervals and consensus sequences: comparison of the resolving power of traditional biostratigraphy and computer-assisted correlation" in *High Resolution Approaches in Paleontology,* P. J. Harries, Ed. (Kluwer-Academic, 2003), pp. 49-94.

20. R. A. Cooper, P. M. Sadler, A. Munnecke, J. S. Crampton, Graptoloid evolutionary rates track Ordovician-Silurian global climate change. *Geol. Mag.* **151**, 349–364 (2014). doi:10.1017/S0016756813000198

21. Y. Wang, P. M. Sadler, S. Z. Shen, D. H. Erwin, Y. C. Zhang, X. D. Wang, W. Wang, J. L. Crowley, C. M. Henderson, Quantifying the process and abruptness of the end-Permian mass extinction. *Paleobiology* **40**, 113–129 (2014). doi:10.1666/13022

22. P. M. Sadler, Quantitative biostratigraphy-achieving finer resolution in global correlation. *Annu. Rev. Earth Planet. Sci.* **32**, 187–213 (2004). doi:10.1146/annurev.earth.32.101802.120428

23. P. M. Sadler, R. A. Cooper, M. J. Melchin, Sequencing the graptoloid clade: Building a global diversity curve from local range charts, regional composites and global time-lines. *Proc. Yorks. Geol. Soc.* **58**, 329–343 (2011). doi:10.1144/pygs.58.4.296

24. K. M. Cohen, S. C. Finney, P. L. Gibbard, J. X. Fan, The ICS International Chronostratigraphic Chart. *Episodes* **36**, 199–204 (2013). doi:10.18814/epiiugs/2013/v36i3/002

25. S. Z. Shen, J. Y. Rong, Eds., *New Advances in the Integrative Stratigraphy and Timescale of China*, vol. 62 of *Science China Earth Sciences* (Science China Press, 2019).

26. M. Foote, Origination and extinction components of taxonomic diversity: Paleozoic and post-Paleozoic dynamics. *Paleobiology* **26**, 578–605 (2000). doi:10.1666/0094-8373(2000)026<0578:OAECOT>2.0.CO;2

27. M. R. Saltzman, C. A. Cowan, A. C. Runkel, B. Runnegar, M. C. Stewart, A. R. Palmer, The Late Cambrian Spice ($\delta^{13}C$) Event and the Sauk II-SAUK III Regression: New Evidence from Laurentian Basins in Utah, Iowa, and Newfoundland. *J. Sediment. Res.* **74**, 366–377 (2004). doi:10.1306/120203740366

28. T. Servais, D. A. T. Harper, The Great Ordovician Biodiversification Event (GOBE): Definition, concept and duration. *Lethaia* **51**, 151–164 (2018). doi:10.1111/let.12259

29. J. Y. Rong, B. Huang, R. B. Zhan, D. A. T. Happer, Latest Ordovician and earliest Silurian brachiopods succeeding the Hirnantia fauna in south-east China. *Spec. Pap. Palaeontology* **90**, 5–142 (2013).

30. G. X. Wang, R. B. Zhan, I. G. Percival, The end-Ordovician mass extinction: A single-pulse event? *Earth Sci. Rev.* **192**, 15–33 (2019). doi:10.1016/j.earscirev.2019.01.023

31. D. M. Raup, J. J. Sepkoski Jr., Mass extinctions in the marine fossil record. *Science* **215**, 1501–1503 (1982). doi:10.1126/science.215.4539.1501 Medline

32. R. K. Bambach, A. H. Knoll, S. C. Wang, Origination, extinction, and mass depletions of marine diversity. *Paleobiology* **30**, 522–542 (2004). doi:10.1666/0094-8373(2004)030<0522:OEAMDO>2.0.CO;2

33. M. E. Clapham, S. Z. Shen, D. J. Bottjer, The double mass extinction revisited: Reassessing the severity, selectivity, and causes of the end-Guadalupian biotic crisis (Late Permian). *Paleobiology* **35**, 32–50 (2009). doi:10.1666/08033.1

34. S. D. Burgess, S. Bowring, S. Z. Shen, High-precision timeline for Earth's most severe extinction. *Proc. Natl. Acad. Sci. U.S.A.* **111**, 3316–3321 (2014). doi:10.1073/pnas.1317692111 Medline

35. J. J. Sepkoski Jr., A factor analytic description of the Phanerozoic marine fossil record. *Paleobiology* **7**, 36–53 (1981). doi:10.1017/S0094837300003778

36. S. Z. Shen, H. Zhang, W. Z. Li, L. Mu, J. F. Xie, Brachiopod diversity patterns from Carboniferous to Triassic in South China. *Geol. J.* **41**, 345–361 (2006). doi:10.1002/gj.1047

37. A. L. Cárdenas, P. J. Harries, Effect of nutrient availability on marine origination rates throughout the Phanerozoic eon. *Nat. Geosci.* **3**, 430–434 (2010). doi:10.1038/ngeo869

38. D. H. Erwin, Climate as a driver of evolutionary change. *Curr. Biol.* **19**, R575–R583 (2009). doi:10.1016/j.cub.2009.05.047 Medline

39. P. J. Mayhew, M. A. Bell, T. G. Benton, A. J. McGowan, Biodiversity tracks temperature over time. *Proc. Natl. Acad. Sci. U.S.A.* **109**, 15141–15145 (2012). doi:10.1073/pnas.1200844109 Medline

40. P. J. Mayhew, G. B. Jenkins, T. G. Benton, A long-term association between global temperature and biodiversity, origination and extinction in the fossil

record. *Proc. Biol. Sci.* **275**, 47–53 (2008). doi:10.1098/rspb.2007.1302 Medline

41. I. P. Montañez, N. J. Tabor, D. Niemeier, W. A. Dimichele, T. D. Frank, C. R. Fielding, J. L. Isbell, L. P. Birgenheier, M. C. Rygel, CO_2-forced climate and vegetation instability during Late Paleozoic deglaciation. *Science* **315**, 87–91 (2007). doi:10.1126/science.1134207 Medline

42. J. A. Trotter, I. S. Williams, C. R. Barnes, C. Lécuyer, R. S. Nicoll, Did cooling oceans trigger Ordovician biodiversification? Evidence from conodont thermometry. *Science* **321**, 550–554 (2008). doi:10.1126/science.1155814 Medline

43. J. A. Trotter, I. S. Williams, C. R. Barnes, P. Männik, A. Simpson, New conodont $\delta^{18}O$ records of Silurian climate change: Implications for environmental and biological events. *Palaeogeogr. Palaeoclimatol. Palaeoecol.* **443**, 34–48 (2016). doi:10.1016/j.palaeo.2015.11.011

44. J. T. Chen, I. P. Montañez, Y. P. Qi, S. Z. Shen, X. D. Wang, Strontium and carbon isotopic evidence for decoupling of pCO_2 from continental weathering at the apex of the late Paleozoic glaciation. *Geology* **46**, 395–398 (2018). doi:10.1130/G40093.1

45. B. Chen, M. M. Joachimski, S. Z. Shen, L. L. Lambert, X. L. Lai, X. D. Wang, J. Chen, D. X. Yuan, Permian ice volume and palaeoclimate history: Oxygen isotope proxies revisited. *Gondwana Res.* **24**, 77–89 (2013). doi:10.1016/j.gr.2012.07.007

46. A. Delabroye, M. Vecoli, The end-Ordovician glaciation and the Hirnantian Stage: A global review and questions about Late Ordovician event stratigraphy. *Earth Sci. Rev.* **98**, 269–282 (2010). doi:10.1016/j.earscirev.2009.10.010

47. S. Finnegan, N. A. Heim, S. E. Peters, W. W. Fischer, Climate change and the selective signature of the Late Ordovician mass extinction. *Proc. Natl. Acad. Sci. U.S.A.* **109**, 6829–6834 (2012). doi:10.1073/pnas.1117039109 Medline

48. M. M. Joachimski, S. Breisig, W. Buggisch, J. A. Talent, R. Mawson, M. Gereke, J. R. Morrow, J. Day, K. Weddige, Devonian climate and reef evolution: Insights from oxygen isotopes in apatite. *Earth Planet. Sci. Lett.* **284**, 599–609 (2009). doi:10.1016/j.epsl.2009.05.028

49. C. Huang, M. M. Joachimski, Y. M. Gong, Did climate changes trigger the Late Devonian Kellwasser Crisis? Evidence from a high-resolution conodont $\delta^{18}O_{PO4}$ record from South China. *Earth Planet. Sci. Lett.* **495**, 174–184 (2018). doi:10.1016/j.epsl.2018.05.016

50. J. Chen, S. Z. Shen, X. H. Li, Y. G. Xu, M. M. Joachimski, S. A. Bowring, D. H. Erwin, D. X. Yuan, B. Chen, H. Zhang, Y. Wang, C. Q. Cao, Q. F. Zheng, L. Mu, High-resolution SIMS oxygen isotope analysis on conodont apatite from South China and implications for the end-Permian mass extinction. *Palaeogeogr. Palaeoclimatol. Palaeoecol.* **448**, 26–38 (2016). doi:10.1016/j.palaeo.2015.11.025

51. M. M. Joachimski, X. L. Lai, S. Z. Shen, H. S. Jiang, G. M. Luo, B. Chen, J. Chen, Y. D. Sun, Climate warming in the latest Permian and the Permian–Triassic mass extinction. *Geology* **40**, 195–198 (2012). doi:10.1130/G32707.1

52. Y. Sun, M. M. Joachimski, P. B. Wignall, C. Yan, Y. Chen, H. Jiang, L. Wang, X. Lai, Lethally hot temperatures during the Early Triassic greenhouse. *Science* **338**, 366–370 (2012). doi:10.1126/science.1224126 Medline

53. M. R. Saltzman, E. Thomas, "Carbon isotope stratigraphy" in *The Geologic Time Scale 2012*, F. M. Gradstein, J. G. Ogg, M. D. Schmitz, G. M. Ogg, Eds. (Elsevier, 2012), vol. 1, pp. 207–232.

54. D. H. Rothman, Thresholds of catastrophe in the Earth system. *Sci. Adv.* **3**, e1700906 (2017). doi:10.1126/sciadv.1700906 Medline

55. T. G. Zhang, Y. N. Shen, R. B. Zhan, S. Z. Shen, X. Chen, Large perturbations of the carbon and sulfur cycle associated with the Late Ordovician mass extinction in South China. *Geology* **37**, 299–302 (2009). doi:10.1130/G25477A.1

56. M. M. Joachimski, R. D. Pancost, K. H. Freeman, C. Ostertag-Henning, W. Buggisch, Carbon isotope geochemistry of the Frasnian-Famennian transition. *Palaeogeogr. Palaeoclimatol. Palaeoecol.* **181**, 91–109 (2002). doi:10.1016/S0031-0182(01)00474-6

57. R. A. Berner, Z. Kothavala, GEOCARB III: A revised model of atmospheric CO_2 over phanerozoic time. *Am. J. Sci.* **301**, 182–204 (2001). doi:10.2475/ajs.301.2.182

58. G. L. Foster, D. L. Royer, D. J. Lunt, Future climate forcing potentially without precedent in the last 420 million years. *Nat. Commun.* **8**, 14845 (2017). doi:10.1038/ncomms14845 Medline

59. C. R. Witkowski, J. W. H. Weijers, B. Blais, S. Schouten, J. S. Sinninghe Damsté, Molecular fossils from phytoplankton reveal secular Pco_2 trend over the Phanerozoic. *Sci. Adv.* **4**, eaat4556 (2018). doi:10.1126/sciadv.aat4556 Medline

60. J. M. McArthur, R. J. Howarth, G. A. Shields, "Strotium isotope stratigraphy" in *The Geological Time Scale 2012*, F. M. Gradstein, J. G. Ogg, M. D. Schmitz, G. M. Ogg, Eds. (Elsevier, 2012), vol. 2, pp. 127–144.

61. J. X. Fan, S. Z. Shen, X. D. Wang, Y. Wang, H. Zhang, X. Chen, G. X. Li, Y. C. Zhang, Y. K. Shi, D. X. Yuan, Q. Chen, L. N. Zhang, Y. Y. Zhao, J. Yang, X. D. Hou, P. M. Sadler, Data and code for: A high-resolution summary of Cambrian to Early Triassic marine invertebrate biodiversity, Version 3, Dryad (2019); https://datadryad.org/stash/dataset/doi:10.5061/dryad.0gb5mkkx1.

62. J. Veizer, A. Prokoph, Temperatures and oxygen isotopic composition of Phanerozoic oceans. *Earth Sci. Rev.* **146**, 92–104 (2015). doi:10.1016/j.earscirev.2015.03.008

63. W. W. Hay, A. Migdisov, A. N. Balukhovsky, C. N. Wold, S. Flogel, E. Soding, Evaporites and the salinity of the ocean during the Phanerozoic: Implications for climate, ocean circulation and life. *Palaeogeogr. Palaeoclimatol. Palaeoecol.* **240**, 3–46 (2006). doi:10.1016/j.palaeo.2006.03.044

64. B. L. M. Hubert, M. Zapalski, J. P. Nicollin, B. Mistiaen, D. Brice, Selected benthic faunas from the Devonian of the Ardennes: An estimation of palaeobiodiversity. *Acta Geol. Pol.* **57**, 223–262 (2007).

65. J. Y. Rong, Z. J. Fang, Z. H. Zhou, R. B. Zhan, X. D. Wang, X. L. Yuan, Eds., *Originations, Radiations and Biodiversity Changes: Evidence from the Chinese Fossil Record* (Science Press, 2006).

66. J. S. Crampton, R. A. Cooper, P. M. Sadler, M. Foote, Greenhouse-icehouse transition in the Late Ordovician marks a step change in extinction regime in the marine plankton. *Proc. Natl. Acad. Sci. U.S.A.* **113**, 1498–1503 (2016). doi:10.1073/pnas.1519092113 Medline

67. F. M. Gradstein, J. G. Ogg, M. D. Schmitz, G. M. Ogg, Eds., *The Geologic Time Scale 2012* (Elsevier, 2012).

68. J. Alroy, Geographical, environmental and intrinsic biotic controls on Phanerozoic marine diversification. *Palaeontology* **53**, 1211–1235 (2010). doi:10.1111/j.1475-4983.2010.01011.x

69. J. Starrfelt, L. H. Liow, How many dinosaur species were there? Fossil bias and true richness estimated using a Poisson sampling model. *Philos. Trans. R. Soc. Lond. B Biol. Sci.* **371**, 20150219 (2016). doi:10.1098/rstb.2015.0219 Medline

70. S. D. Burgess, J. D. Muirhead, S. A. Bowring, Initial pulse of Siberian Traps sills as the trigger of the end-Permian mass extinction. *Nat. Commun.* **8**, 164 (2017). doi:10.1038/s41467-017-00083-9 Medline

71. S. Z. Shen, H. Zhang, Y. C. Zhang, D. X. Yuan, B. Chen, W. H. He, L. Mu, W. Lin, W. Q. Wang, J. Chen, Q. Wu, C. Q. Cao, Y. Wang, X. D. Wang, Permian integrative stratigraphy and timescale of China. *Sci. China Earth Sci.* **62**, 154–188 (2019). doi:10.1007/s11430-017-9228-4

72. J. Aldrich, Correlations genuine and spurious in Pearson and Yule. *Stat. Sci.* **10**, 364–376 (1995). doi:10.1214/ss/1177009870

73. A. C. Scotese, T. Moore, *Atlas of Phanerozoic Temperatures (Mollweide Projection)*, vols. 1–6 of *PALEOMAP Project PaleoAtlas for ArcGIS* (PALEOMAP Project, 2014).

74. C. R. Fielding, T. D. Frank, J. L. Isbell, "The Late Paleozoic ice age: A review of current understanding and synthesis of global climate patterns" in C. R. Fielding, T. D. Frank, J. L. Isbell, Eds., *Resolving the Late Paleozoic Ice Age in Time and Space* (Geological Society of America, 2008), vol. 441, pp. 343–354.

75. K. Roy, D. Jablonski, J. W. Valentine, Higher taxa in biodiversity studies: Patterns from eastern Pacific marine molluscs. *Philos. Trans. R. Soc. Lond. B Biol. Sci.* **351**, 1605–1613 (1996). doi:10.1098/rstb.1996.0144

76. A. Z. Krug, D. Jablonski, J. W. Valentine, Species-genus ratios reflect a global history of diversification and range expansion in marine bivalves. *Proc. Biol. Sci.* **275**, 1117–1123 (2008). doi:10.1098/rspb.2007.1729 Medline